Chemical Engineering Journal 156 (2010) 360–365

Contents lists available at ScienceDirect

Chemical Engineering Journal

journal homepage: www.elsevier.com/locate/cej

Quantitative design of seed load for solution cooling crystallization based on kinetic analysis

D.C. Huang[a,b], W. Liu[c], S.K. Zhao[a], Y.Q. Shi[a], Z.X. Wang[a,*], Y.M. Sun[b]

[a] Department of Pharmaceutical Engineering, China Pharmaceutical University, # 24 Tongjiaxiang, Nanjing 210009, PR China
[b] Department of Chemistry and Chemical Engineering, Southeast University, Nanjing 210096, PR China
[c] Department of Mechanical Electronics Engineering, Nanjing Normal University, Nanjing 210042, PR China

ARTICLE INFO

Article history:
Received 17 May 2009
Received in revised form
19 September 2009
Accepted 20 September 2009

Keywords:
Solution cooling crystallization
Product size distribution
Kinetic analysis
Seed load
Quantitative design

ABSTRACT

Seed load of crystallization has a direct effect on the product qualities. To further reveal the effects of seed load on crystallization kinetics and improve the product size distribution, the aqueous solution of potassium nitrate (KNO_3–H_2O) is employed as a model system and the relevant kinetic experiments are conducted in a batch cooling crystallizer. The crystal nucleation and growth rate parameters are firstly estimated with the concentration and transmittance data using a mathematical model reported in our lab, and then the backward calculations with the help of the model parameters are successfully performed. It is found that the nucleation capacity decreases and growth capacity increases with increasing seed load, and the size distribution of crystal products tends to be more uniform. However, with the increasing of seed load, the linear growth rate of single crystal and the mean size of products both reduce accordingly. Based on the calculational and experimental results, a quantitative design scheme concerning seed load is proposed by further kinetic analyses, and the corresponding verification experiments are carried out. The results show that under the guidance of the proposed scheme, the size distribution of crystal products is more concentrated and the mean size of final particles can also escape from reducing obviously.

1. Introduction

Solution cooling crystallization is a widely used industrial separation technology, but there still exist many problems in its operation optimization due to the complicated process mechanism.

In order to increase the mean size of crystal products and improve crystal size distribution (CSD), as reviewed in the recent literature [1–6], lots of operation policies such as optimized cooling profile and controlled supersaturation degree of system have been put forward. Among them, the method of loading seeds is of high effectiveness and is broadly applied in industrial production. Being different from the case of unseeded crystallization, the seeded crystallization process usually has lower nucleation rate and better CSD of products. This is because the most of solute molecules in solution will be precipitated on the seed surfaces when seeds are loaded.

In 1925, Griffiths [7] first investigated the seeded crystallization process and presented the operation strategy of loading seeds to control the amount of nucleation and CSD of products. In 1934, Ting and McCabe [8] proved that under the low supersaturation degree, loading seeds can restrain the formation of new nucleus in most salt systems. In 1999, Doki et al. [9] found that if the seed load is more than a critical value, the uniform size crystals can be obtained in the batch cooling crystallization experiments of potassium alum. In 2004, Loï Mi Lung-Somarriba et al. [10] investigated the influence of seed surface area on the CSD in the glycine batch cooling system, indicating that the CSD can be controlled when the seed surface area is over a specific value. Besides, Chung et al. [11] also studied the relationship between seed size and product particle characteristics for cooling crystallization. The above mentioned and other similar works [12–17] all manifested that loading seeds or not, seed load, seed size, etc., can directly impact the qualities of final crystal products.

Most of literature researches paid great attention to disclosing the effect of seed load on nucleation kinetics, but little attention was paid to discussing the effect of seed load on crystal growth kinetics, and the satisfying quantitative evaluation concerning seed load has not yet been really realized. The present work is to further reveal the seed load influence on the process kinetics of solution cooling crystallization, particularly crystal growth kinetics, and thus put forward a quantitative design scheme for seed loading, in which the KNO_3–H_2O solution, a typical model system in crystallization researches is employed, and the relevant kinetic experiments and analyses are performed.

* Corresponding author. Tel.: +86 25 83244816; fax: +86 25 83271258.
E-mail address: wzxcpu@yahoo.cn (Z.X. Wang).

1385-8947/$ – see front matter © 2009 Elsevier B.V. All rights reserved.
doi:10.1016/j.cej.2009.09.029

Nomenclature

b	nucleation rate parameter
B	secondary nucleation rate (# $cm^{-3}\,min^{-1}$)
c	concentration ($g\,g^{-1}$)
c_0	initial concentration ($g\,g^{-1}$)
c_{sat}	saturation concentration ($g\,g^{-1}$)
dl	increment of crystal size in dt time interval (cm)
$f(L,t)$	function of CSD
g	growth rate parameter
G	linear growth rate of single crystal ($cm\,min^{-1}$)
k_α	surface shape factor
k_b	nucleation rate parameter ($g\,cm^{-6}\,min^{-1}$)
k_B	nucleation rate parameter ($g\,cm^{-3}\,min^{-1}$)
k_g	growth rate parameter ($cm\,min^{-1}$)
k_v	volume shape factor
L	crystal characteristic size (cm)
L_0	characteristic size of nucleation (cm)
m_L	solvent mass (g)
m_S	seed load (g)
r	transmittance
S	relative supersaturation
t	crystallization time (min)
V	solution volume (cm^3)
V_c	total volume of crystals in system (cm^3)
w	transmittance flow-cell width (cm)
X_B	nucleation capacity ($g\,min^{-1}$)
X_G	growth capacity ($g\,min^{-1}$)

Greek symbols

μ_2	the second moment of CSD function ($cm^2\,cm^{-3}$)
μ_j	the jth moment of CSD function ($cm^j\,cm^{-3}$)
$\hat{\mu}_3$	the third moment of CSD function ($cm^3\,g^{-1}$)
ρ_0	initial density of solution ($g\,cm^{-3}$)
ρ_c	crystal density ($g\,cm^{-3}$)

Subscripts

c	solid phase
0	initial state
sat	saturated state

2. Kinetic model

Based on the assumption that the characteristic diameters of newly generated nuclei are of the same size L_0 [18–20], with the help of Beer–Lambert law, McCabe's ΔL law and population balance theory [20,21], a kinetic model for batch cooling crystallization was established in our prior work [22] by assuming the homogeneous mixture of system and ignoring the breakage and agglomeration of crystal particles. The derivation of this model is provided by Appendix A, and the model equation can be written as

$$-m_L\frac{dc}{dt} = \frac{m_L(1+c_0)[(c_0-c)+(m_S/m_L)]}{\rho_0}k_B\left(\frac{c-c_{sat}}{c_{sat}}\right)^b + \frac{6m_L(1+c_0)k_v\rho_c(-\ln r)}{k_\alpha w\rho_0}k_g\left(\frac{c-c_{sat}}{c_{sat}}\right)^g \quad (1)$$

where k_α and k_v represent the surface shape factor and volume shape factor of crystal particles, respectively. For KNO_3 crystal, k_α and k_v are about 6 and 1, respectively. ρ_c is the crystal density, and its value is about 2.11 $g\,cm^{-3}$ for KNO_3 crystal at 20 °C [20].

In Eq. (1), the two terms on the right side of equal mark can orderly represent the nucleation capacity and growth capacity of crystallization system. In order to be convenient for description, it is essential to separately define the two terms by variables X_B and X_G, namely

$$X_B = \frac{m_L(1+c_0)[(c_0-c)+(m_S/m_L)]}{\rho_0}k_B\left(\frac{c-c_{sat}}{c_{sat}}\right)^b \quad (2)$$

$$X_G = \frac{6m_L(1+c_0)k_v\rho_c(-\ln r)}{k_\alpha w\rho_0}k_g\left(\frac{c-c_{sat}}{c_{sat}}\right)^g \quad (3)$$

where X_B and X_G denote the nucleation capacity and growth capacity of crystallization system, respectively.

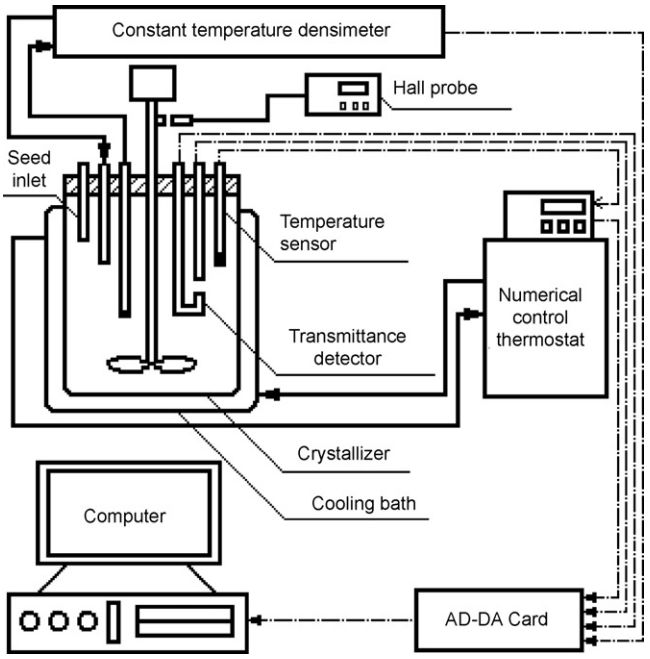

Fig. 1. Schematic diagram of experimental apparatus for seeded batch cooling crystallization.

3. Experiments

3.1. Experimental apparatus

The schematic diagram of experimental apparatus is shown in Fig. 1. Experiments are performed in a 600 ml glass jacket crystallizer with a blade stirrer. The rotating speed of stirrer is hold at about 750 r min^{-1} to ensure well-mixed crystal suspension. The temperature of crystallizer is controlled by a numerical control thermostat, and the concentration of crystallization solution is determined real-timely by using a densimeter introduced by Wu et al. [23] and Qiu and Rasmuson [24]. The transmittance is obtained by a set of transmittance detector with the laser light wavelength of 680 nm and the flow-cell width w of 2.26 cm, and its specific working principle can refer to the literature [20,23]. All experimental data, e.g., temperatures, densities, concentrations and transmittances, are automatically collected and stored by PC every 3 s.

3.2. Experimental parameter conditions

Four runs of seeded crystallization experiments on KNO_3–H_2O solution are designed. The initial solution concentration c_0, the mass ratio of KNO_3 to H_2O, is 0.2614 $g\,g^{-1}$, and the corresponding solution density ρ_0 and saturation temperature are 1.1284 $g\,cm^{-3}$ and 15 °C, respectively. The cooling rate is set at 0.04 °C min^{-1}. The seed load m_S and solution mass of each run are listed in Table 1. In these runs, the seeds are sampled by international standard sieve mesh and the relevant sizes are between 0.35 and 0.42 mm.

Table 1
Values of seed load and solution mass in each experiment.

Run no.	Seed load (g)	Solution mass (g)
1	2.1937	620.0602
2	3.3171	620.0307
3	5.3372	620.0787
4	6.9214	620.0496

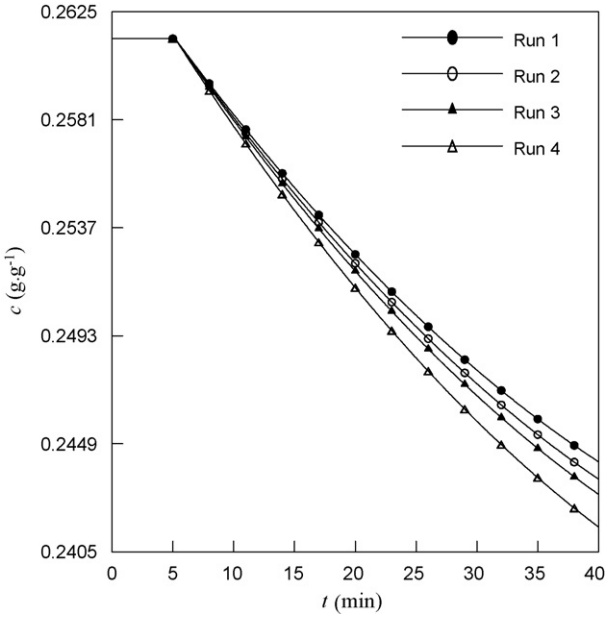

Fig. 2. Concentration versus time profiles fitted with experimental data (the initial solution concentration (0.2614 g g^{-1}) and cooling rate (0.04 °C min^{-1}) are constant).

4. Results and discussion

4.1. Concentration and transmittance

The fitted profiles of concentration c versus time t are illustrated in Fig. 2, and the transmittance r profiles are shown in Fig. 3. It can be found that both concentration and transmittance start to decrease at about 5 min, implying that the supersaturated solution in metastable zone is induced to generate solute precipitation by artificial loading seeds. From Figs. 2 and 3, we also know that the concentration and transmittance both drop more distinctly with the increasing of seed load.

4.2. Nucleation and growth rate parameters

Based on the experimental data of concentration and transmittance, and the known data such as saturation concentration c_{sat} [20] and solvent mass m_L, the nucleation rate parameters, k_B and b, and growth rate parameters, k_g and g, of each run can be estimated with Eq. (1) by multivariate nonlinear regression of Gauss–Newton method, where the first-order derivative of concentration c with respect to time t can be calculated by cubic spline method. The results are listed in Table 2. For comparison, the literature [20] values are also presented.

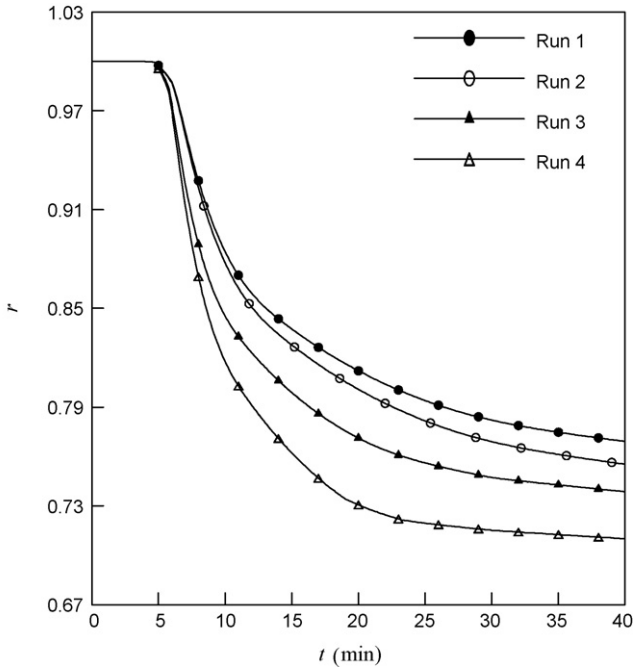

Fig. 3. Transmittance versus time profiles fitted with experimental data (the initial solution concentration (0.2614 g g^{-1}), cooling rate (0.04 °C min^{-1}) and flow-cell width (2.26 cm) are constant).

As far as the general deviation of crystallization kinetics calculation is concerned, according to Table 2, it is obvious that the fitted parameter results not only agree well with those reported in the literature, but the correlation coefficients are higher and the confidence intervals are narrower. Therefore, we can conclude that the fitting of model versus data is remarkable and the parameter results are credible.

4.3. Nucleation and growth capacities

By using the present data of nucleation and growth rate parameters, concentration and transmittance, the nucleation capacity X_B and the growth capacity X_G can be calculated by Eqs. (2) and (3), respectively. The variations of X_B and X_G versus time are plotted in Fig. 4, showing that X_B in each run is continuously decreasing with the prorogating of time, due to the reduction of supersaturation. On the other hand, X_G is gradually increasing even with the dropping of supersaturation degree, due to the increasing of the total particle population in system. The variation characteristics of X_B and X_G, to a great extent, confirm that the solution crystallization is a separation process with a stage-transformation, i.e., from nucleation dominated to growth dominated [19].

Fig. 4 also shows that, with the seed load increasing, the nucleation capacity decreases and the growth capacity increases. As the

Table 2
Values of crystal nucleation and growth rate parameters ($L_0 \approx 0.005$ cm).

Run no.	k_B (g cm^{-3} min^{-1})	b	k_g (cm min^{-1})	g	Correlation coefficient
1	0.736 ± 0.481	1.438 ± 0.369	0.907 ± 0.402	1.712 ± 0.927	0.926
2	1.141 ± 0.383	2.201 ± 0.191	0.218 ± 0.117	1.359 ± 0.364	0.943
3	0.483 ± 0.407	1.054 ± 0.874	0.884 ± 0.362	1.892 ± 0.828	0.908
4	0.204 ± 0.126	0.903 ± 0.505	0.425 ± 0.106	1.767 ± 0.683	0.924
Literature values [20]	0.26[a]	2.25	0.15	1.5	–

[a] In literature [20], $k_b = 2.11 \times 10^6$ g cm^{-6} min^{-1}.

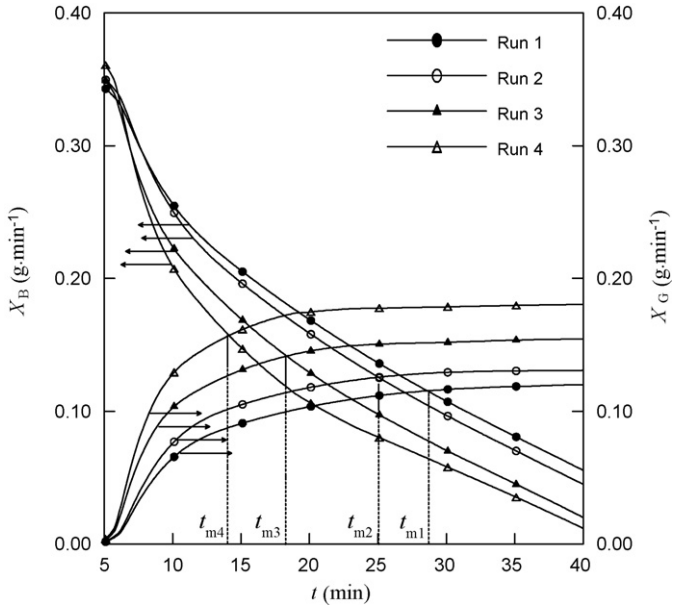

Fig. 4. Nucleation and growth capacities versus time curves obtained by backward calculations with Eqs. (2) and (3) (X_B and X_G represent the nucleation and growth capacity separately, the parameter values of k_B, b, k_g and g are listed in Table 2, the experimental data of concentration c and transmittance r are shown in Figs. 2 and 3, respectively).

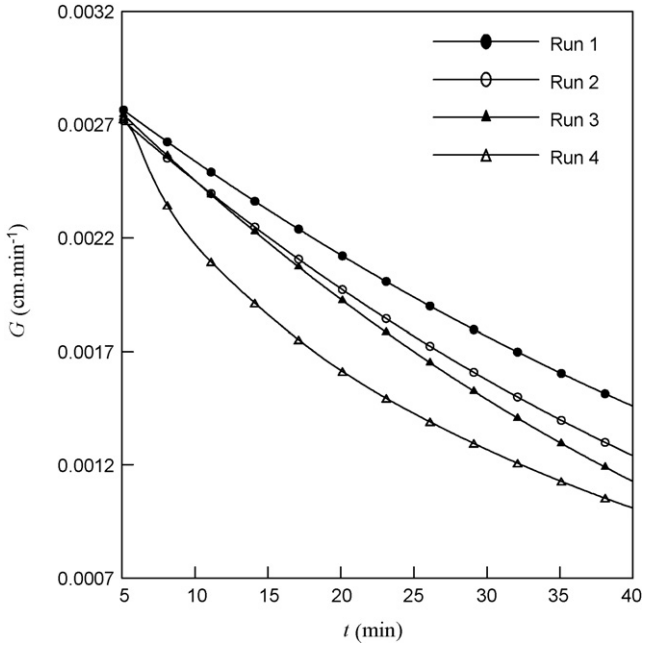

Fig. 5. Crystal linear growth rate versus time curves obtained by backward calculation with Eq. (4) (G represents the linear growth rate of single crystal, the parameter values of k_g and g are listed in Table 2, the experimental data of concentration c is shown in Fig. 2, the data of saturation concentration c_{sat} is reported in the literature [20]).

more seeds can supply the more surface area of particles, more solute molecules can be precipitated on these surfaces, enhancing the growth capacity and thus weakening the nucleation capacity accordingly. Form the report [9], to achieve more uniform size crystals, the nucleation capacity should be restrained while the growth capacity should be enhanced. Hence, the strategy of increasing seed load is recommended for the better CSD of products.

Table 3 summaries the data of product particle sizes in the four runs with the same cooling time. As can be seen, under the higher seed load, the product sizes are more concentrated in certain or several adjacent zones, and the size distribution of final particles is more uniform. This is in accord with the above mentioned conclusion that the nucleation capacity decreases and growth capacity increases with a rise of the seed load.

4.4. Linear growth rate of crystal

The linear growth rate of crystal, G, is also an important parameter to characterize the process kinetics of crystallization operation, since its value represents the increasing rate of single crystal size. As far as KNO_3–H_2O system is concerned, the crystal growth behavior approximately obeys McCabe's ΔL law [20], thus the different size particles have the similar linear growth rate and the rate value can be calculated by

$$G = k_g \left(\frac{c - c_{sat}}{c_{sat}} \right)^g \quad (4)$$

Table 4
Data information of critical point that distinguishes nucleation dominated stage from growth dominated stage.

Run no.	t_{mi} (min)	$c_{t_{mi}}$ (g g^{-1})	$m_{t_{mi}}$ (g)
1	28.5	0.2487	8.4366
2	25.1	0.2496	9.1721
3	18.3	0.2529	9.5440
4	14.0	0.2550	10.1608

The curves of G versus time are illustrated in Fig. 5. As shown, the rate G gradually decreases in the crystallization process. This is because the operation selected a relative low cooling rate, the solution supersaturation produced by temperature decreasing was less than that consumed by solute precipitation, causing a drop of the supersaturation degree and thus decreasing the growth rate.

Fig. 5 also indicates, being different from the case of the growth capacity X_G, the linear growth rate G decreases with a rise of the seed load, probably due to the more seeds increasing the particle population in system. Too many particles reinforce the competition of adsorbing solute molecules, limiting the rapid growth of single crystal and reducing the mean size of products. As shown in Table 3, the mass fractions of crystal products whose size is equal or larger than 0.85 mm are 0.367, 0.257, 0.165 and 0.106 in the four runs, respectively. The degression shows that the higher seed load, the lower mean size of final products in a limitation operation time.

Table 3
Size information of crystal products without seed load optimization.

Run no.	Mass fraction						
	Crystal sizes (mm)						Mass of crystal products (g)
	<0.35	0.35–0.50	0.50–0.71	0.71–0.85	0.85–1.0	>1.0	
1	0.139	0.174	0.148	0.172	0.286	0.081	10.7638
2	0.104	0.116	0.208	0.315	0.212	0.045	13.0175
3	0.056	0.169	0.364	0.246	0.134	0.031	14.4596
4	0.043	0.287	0.395	0.169	0.106	–	17.0214

Table 5
Size information of crystal products after seed load optimization.

Run no.	Mass fraction					
	Crystal sizes (mm)					Mass of crystal products (g)
	<0.50	0.50–0.71	0.71–0.85	0.85–1.0	>1.0	
1′	0.014	0.309	0.512	0.143	0.022	11.3327
2′	0.018	0.417	0.443	0.109	0.013	13.8641
3′	0.022	0.474	0.417	0.087	–	15.0165
4′	0.027	0.546	0.378	0.049	–	17.9518

4.5. Quantitative design of seed load

4.5.1. The design basis and idea

According to the above kinetic analyses and calculations, the seed load should be increased as much as possible to improve the size distribution of products. However, the more seeds could also restrain the growth rate of single crystal and reduce the mean size of products, so the seed load should be optimized.

As shown in Fig. 4, with the operation proceeding, the curve of nucleation capacity is monotonously decreasing and the curve of growth capacity is monotonously increasing in each run, there exists an intersection point of two curves. If orderly define the abscissa value of these points as t_{m1}, t_{m2}, t_{m3} and t_{m4} for the four runs, it is obvious that when the operation was in the left zone of intersection point, the nucleation capacity was stronger than the growth capacity, and when the operation was in the right zone of intersection point, the growth capacity was stronger than the nucleation capacity, thus the intersection point represents the critical point that distinguishes the nucleation dominated stage from the growth dominated stage. That is to say, when the crystallization operation proceeded up to the moment of t_{m1}, t_{m2}, t_{m3} or t_{m4}, a dynamic population balance of crystal particles had been built in system, then the number of particles no longer increased greatly and most of solute molecules would be precipitated on the surfaces of particles already existed, i.e., the crystallization operation started to be shifted from the nucleation dominated stage to the growth dominated stage. Hence, we conjecture, for a newly prepared KNO_3–H_2O solution whose initial concentration equals that of intersection point, as seeds loaded equals the amount of crystals accumulated in system at the intersection point time, the nucleation dominated stage may be avoided and the growth dominated stage will be introduced directly under the same cooling rate as before. Accordingly, more uniform size products will be obtained, and the mean size of final particles may also escape from reducing remarkably since the seed load is limited but not overdosed without guidance.

4.5.2. The example

For example, when the $t_{m1}\approx 28.5$ min, as seen from Fig. 2, the corresponding concentration value of $c_{t_{m1}}$ is about 0.2487 g g^{-1}, thus the accumulated crystal mass $m_{t_{m1}}$ in system can be calculated as follows:

$$m_{t_{m1}} = m_{L1}(c_0 - c_{t_{m1}}) + m_{S1} \approx \frac{620.0602}{1+0.2614} \times (0.2614 - 0.2487) + 2.1937 = 8.4366(\mathrm{g}) \quad (5)$$

Similarly, for the second, third and fourth run, the relative values of t_{mi}, $c_{t_{mi}}$ and $m_{t_{mi}}$ (i = 2, 3, 4) can also be calculated, and the relevant results are listed in Table 4.

Based on the seed load design in Section 4.5.1, for the newly prepared experimental solution with initial concentration of $c_{t_{mi}}$ (i = 1, 2, 3, 4), the loading mass of seeds $m_{t_{mi}}$ can be found in Table 4, and the corresponding experimental results are summarized in Table 5. It should be noted that, in the four new experiments, the operating parameters, such as seed size, cooling rate, stirring rate, and so on, are scheduled the same as before, while the time interval is shortened and set at $(40 - t_{mi})$ min.

Comparison between Tables 5 and 3 indicates that when the seeds are loaded quantitatively, the size distribution of products is more concentrated, and the particle mean size does not also reduce obviously. This implies the above quantitative method of seed load could be effective and accessible.

5. Conclusions

For batch cooling crystallization with seed, employing the potassium nitrate aqueous solution as a model system and on the basis of kinetic experiments and simulations, this study confirms that with an increase of seed load, the nucleation capacity decreases and growth capacity increases, and the size distribution of crystal products tends to be more uniform, but meanwhile the linear growth rate of single crystal and the mean size of products both reduce. Based on it, a quantitative design scheme concerning seed load is put forward by further kinetic analyses to optimize the operation, and its effectiveness is gained the preliminary identification from experiments.

Acknowledgments

The authors are grateful to the financial support of the National Key Project on Basic Science (2007CB936300). Simultaneously, we would like to express the special thanks to Prof. Pei Huang for valuable discuss and support.

Appendix A.

The foundation to build the model of Eq. (1) is the mass balance calculation of solute in both liquid and solid phases, i.e., the amount of solute decreasing in liquid phase equaling the summation of new nucleation mass and new growth mass of exiting crystals, and the corresponding equation can be shown by

$$-m_L \frac{dc}{dt} = X_B + X_G \quad (6)$$

The nucleation capacity X_B is the product of the crystal density and the total volume of newly generated nuclei in the system per unit time. Based on the assumption that the characteristic diameters of newly generated nuclei are of the same size L_0 [18–20], the X_B can be expressed by

$$X_B = \rho_c k_v L_0^3 B V \quad (7)$$

For the crystallization of limited cooling interval, the crystal slurry volume V can be approximately calculated by [20]

$$V \approx \frac{m_L(1+c_0)}{\rho_0} \quad (8)$$

Defining the jth moment of crystal size distribution (CSD) function $f(L,t)$ as follows:

$$\mu_j = \int_{L_0}^{+\infty} f(L,t)L^j \,\mathrm{d}L \tag{9}$$

The secondary nucleation rate B can be described by empirical law or correlated with the relative supersaturation and the third moment of $f(L,t)$ on the basis of unit mass solvent [25,26]:

$$B = k_\mathrm{b} S^\mathrm{b} \hat{\mu}_3 \tag{10}$$

the relative supersaturation S is defined by

$$S = \frac{c - c_\mathrm{sat}}{c_\mathrm{sat}} \tag{11}$$

In view of the physical meaning of $\hat{\mu}_3$, $k_v\hat{\mu}_3$ is the total volume of crystal particles in the crystallization system. Thus, the mass balance of solute can be obtained:

$$m_\mathrm{L}(c_0 - c) + m_\mathrm{S} = m_\mathrm{L}\rho_\mathrm{c}k_\mathrm{v}\hat{\mu}_3 \tag{12}$$

From Eq. (12), $\hat{\mu}_3$ can be expressed by

$$\hat{\mu}_3 = \frac{(c_0 - c) + (m_\mathrm{S}/m_\mathrm{L})}{k_\mathrm{v}\rho_\mathrm{c}} \tag{13}$$

Substituting Eqs. (8), (10), (11) and (13) into Eq. (7) and supposing $k_\mathrm{B} = k_\mathrm{b}L_0^3$, we can obtain Eq. (2) of calculating the nucleation capacity X_B. It is noted that, just as k_b, the new variable k_B can also be regarded as the nucleation kinetics parameter, due to L_0 being approximately constant in a certain system crystallization.

Similarly, the crystal growth capacity X_G in Eq. (6) is the product of the crystal density and the total volume of newly grown crystals in the system per unit time, and it can be shown by

$$X_\mathrm{G} = \rho_\mathrm{c}\frac{\mathrm{d}V_\mathrm{c}}{\mathrm{d}t} \tag{14}$$

where V_c is the total volume of all crystals in the system, and it generally can be given as follows [20]:

$$V_\mathrm{c} = Vk_\mathrm{v}\int_{L_0}^{+\infty} f(L,t)L^3 \,\mathrm{d}L \tag{15}$$

During crystallization, the volume V_c increases with the growth of crystals. In an infinitesimal time interval dt, the value of the characteristic size L will change to $L + \mathrm{d}l$ while the variation of CSD function $f(L,t)$ can be neglected [27,28]. Therefore, the first-order derivative of volume V_c with respect to time t can be obtained:

$$\frac{\mathrm{d}V_\mathrm{c}}{\mathrm{d}t} = Vk_\mathrm{v}\int_{L_0}^{+\infty} 3f(L,t)L^2\frac{\mathrm{d}l}{\mathrm{d}t}\,\mathrm{d}L \tag{16}$$

where $\mathrm{d}l/\mathrm{d}t$ is the so-called crystal linear growth rate G, which can also be described by empirical expression [25,26]:

$$\frac{\mathrm{d}l}{\mathrm{d}t} = G = k_\mathrm{g}S^\mathrm{g} \tag{17}$$

Substituting Eq. (17) into Eq. (16) and assuming that the different size crystals have the similar linear growth rate, namely that the crystal growth behavior obeys McCabe's ΔL law [20,21], we can rewrite Eq. (16) as follows:

$$\frac{\mathrm{d}V_\mathrm{c}}{\mathrm{d}t} = 3Vk_\mathrm{v}k_\mathrm{g}S^\mathrm{g}\int_{L_0}^{+\infty} f(L,t)L^2\,\mathrm{d}L \tag{18}$$

The integration term in Eq. (18) is the second moment μ_2 of $f(L,t)$ and $k_\alpha\mu_2$ is the total surface area of crystals on the basis of unit volume slurry at time t [20,29]. According to Beer–Lambert law, the laser transmittance is directly related with the total surface area of crystals [20,26]:

$$\int_{L_0}^{+\infty} f(L,t)L^2\,\mathrm{d}L = \mu_2 = -\frac{2\ln r}{k_\alpha w} \tag{19}$$

Substituting Eqs. (8), (18) and (19) into Eq. (14), we can obtain Eq. (3) of calculating the growth capacity X_G.

Substituting Eqs. (2) and (3) into Eq. (6), we can obtain the kinetic model of Eq. (1).

References

[1] S.M. Nowee, A. Abbas, J.A. Romagnoli, Optimization in seeded cooling crystallization: a parameter estimation and dynamic optimization study, Chem. Eng. Process. 46 (2007) 1096–1106.
[2] W. Paengjuntuek, A. Arpornwichanop, P. Kittisupakorn, Product quality improvement of batch crystallizers by a batch-to-batch optimization and nonlinear control approach, Chem. Eng. J. 139 (2008) 344–350.
[3] Q. Hu, S. Rohani, D.X. Wang, A. Jutan, Optimal control of a batch cooling seeded crystallizer, Powder Technol. 156 (2005) 170–176.
[4] D.B. Patience, P.C. Dell'Orco, J.B. Rawlings, Optimal operation of a seeded pharmaceutical crystallization with growth-dependent dispersion, Org. Proc. Res. Dev. 8 (2004) 609–615.
[5] Q. Hu, S. Rohani, A. Jutan, Modelling and optimization of seeded batch crystallizers, Comput. Chem. Eng. 29 (2005) 911–918.
[6] W. Paengjuntuek, P. Kittisupakorn, A. Arpornwichanop, On-line dynamic optimization integrated with generic model control of a batch crystallizer, J. Ind. Eng. Chem. 14 (2008) 442–448.
[7] H. Griffiths, Mechanical crystallization, J. Soc. Chem. Ind. 44 (1925) 7T–18T.
[8] H.H. Ting, W.L. McCabe, Supersaturation and crystal formation in seeded solutions, Ind. Eng. Chem. 26 (1934) 1201–1207.
[9] N. Doki, N. Kubota, A. Sato, M. Yokota, Scale up experiments on seeded batch cooling crystallization of potassium alum, AIChE J. 45 (1999) 2527–2533.
[10] B. Loï Mi Lung-Somarriba, M. Moscosa-Santillan, C. Porte, A. Delacroix, Effect of seeded surface area on crystal size distribution in glycine batch cooling crystallization: a seeding methodology, J. Cryst. Growth 270 (2004) 624–632.
[11] S.H. Chung, D.L. Ma, R.D. Braatz, Optimal seeding in batch crystallization, CSChE 77 (1999) 590–596.
[12] N. Kubota, N. Doki, M. Yokota, A. Sato, Seeding policy in batch cooling crystallization, Powder Technol. 121 (2001) 31–38.
[13] J.D. Ward, D.A. Mellichamp, M.F. Doherty, Choosing an operating policy for seeded batch crystallization, AIChE J. 52 (2006) 2046–2054.
[14] R. Aldaco, A. Garea, A. Irabien, Modeling of particle growth: application to water treatment in a fluidized bed reactor, Chem. Eng. J. 134 (2007) 66–71.
[15] N. Doki, N. Kubota, A. Sato, M. Yokota, Effect of cooling mode on product crystal size in seeded batch crystallization of potassium alum, Chem. Eng. J. 81 (2001) 313–316.
[16] R. Aldaco, A. Garea, A. Irabien, Calcium fluoride recovery from fluoride wastewater in a fluidized bed reactor, Water Res. 41 (2007) 810–818.
[17] G.P. Zhang, S. Rohani, On-line optimal control of a seeded batch cooling crystallizer, Chem. Eng. Sci. 58 (2003) 1887–1896.
[18] D.C. Huang, Z.X. Wang, W. Liu, Y.M. Sun, New algorithm of kinetic model for solution batch crystallization, Acta Chim. Sin. 64 (2006) 906–910.
[19] P. Huang, D.C. Huang, N.P. Xu, J. Shi, Quantitative identification of nucleation and crystal growth stages in batch crystallization from solution, Chem. J. Chin. Univ. 25 (2004) 504–508.
[20] S.M. Miller, Modelling and quality control strategies for batch cooling crystallizers, Ph.D. Thesis, University of Texas at Austin, 1993.
[21] W.L. McCabe, J.C. Smith, Unit Operations of Chemical Engineering, McGraw-Hill Press, New York, 1956.
[22] D.C. Huang, Z.X. Wang, W. Liu, Y.M. Sun, Kinetics modeling for intermediate and final stages of unseeded crystallization, Acta Chim. Sin. 64 (2006) 611–616.
[23] C. Wu, P. Huang, D.C. Huang, H.Q. Yang, N.P. Xu, J. Shi, Crystallization kinetics of batch spontaneous nucleation of potassium nitrate, Chin. J. Chem. Eng. 13 (2005) 589–595.
[24] Y.F. Qiu, A.C. Rasmuson, Estimation of crystallization kinetics from batch cooling experiments, AIChE J. 40 (1994) 799–812.
[25] S.H. Chung, D.L. Ma, R.D. Braatz, Optimal experimental design in batch crystallization, Chemom. Intell. Lab. Syst. 50 (2000) 83–90.
[26] H.B. Matthews, S.M. Miller, J.B. Rawlings, Model identification for crystallization: theory and experimental verification, Powder Technol. 88 (1996) 227–235.
[27] J. Nyvlt, The effect of the cooling method on the crystal size distribution of the product from a batch crystallizer, Coll. Czech. Chem. Commun. 39 (1974) 3463–3472.
[28] C. Mayer, R. Lacmann, Secondary nucleation of sodium chlorate studied with the aid of asymmetric crystallization, Chem. Eng. Technol. 20 (1997) 633–640.
[29] J.W. Mullin, Crystal size and size distribution: the role of test sieving, Anal. Proc. 30 (1993) 455–456.